Available online at www.sciencedirect.com
ScienceDirect
Journal of the European Ceramic Society 31 (2011) 1049–1056
www.elsevier.com/locate/jeurceramsoc

Original Article

Micro powder injection moulding of alumina micro-channel part

Junhu Meng [a,*], Ngiap Hiang Loh [a], Gang Fu [a,b], Bee Yen Tay [c], Shu Beng Tor [a,b]

[a] School of Mechanical and Aerospace Engineering, Nanyang Technological University, 50 Nanyang Avenue, Singapore 639798, Singapore
[b] Singapore-MIT Alliance (SMA), N3.2-01-36, 65 Nanyang Drive, Singapore 637460, Singapore
[c] Singapore Institute of Manufacturing Technology, 71 Nanyang Drive, Singapore 638075, Singapore

Received 30 August 2010; received in revised form 14 November 2010; accepted 28 November 2010
Available online 11 January 2011

Abstract

A feedstock consisting of submicron alumina powder and a formulated binder, was developed to fabricate alumina micro-channel part by micro powder injection moulding. During small scale-mixing, the mixing torques of feedstocks with four different powder loadings were used to establish a suitable powder loading. The thermal and rheological properties of the selected feedstock were examined and used to establish conditions for large scale mixing, debinding and injection moulding. The micro-channel parts were pressureless sintered at different temperatures. The results showed that the moulded, debound and sintered micro-channel parts had good shape retention. The dimensions of the micro-channel part changed with the different processing steps. High densification of the micro-channel parts was achieved at sintering temperatures of 1350 °C and above. Above 1350 °C, the grain grew significantly with increasing the sintering temperatures and thus it led to a decrease in the microhardness.

Keywords: Al_2O_3; Micro-channel part; Injection moulding; Sintering

1. Introduction

Powder injection moulding (PIM) is an established mass-production process for manufacturing complex metal and ceramic parts. In the last few years ago, there is growing interest in the micro PIM process for fabricating micro-components. Micro-components can be classified into three categories: micro-parts, microstructured components and micro-precision parts.[1] Micro-parts are generally understood to be single or separated components with outer dimensions in the range of a few millimeters, but having details in the sub-millimeter range. Microstructured components have outer dimensions of several millimeters up to a few centimeters with three-dimensional micro-structures being located on one or several surface areas. There is great potential for metal and ceramic micro PIM parts and microstructured components in various fields of application and important market opportunities such as medical technology, micro-system technology, micro-fluidics, micro-sensors and micro-mechanics.[2]

As in PIM, the four main processing steps of micro PIM are: mixing, injection moulding, debinding and sintering. In the mixing step, a binder is mixed with the metal or ceramic powder to form a mixture known as the feedstock. The feedstock is pelletized into suitable size for injection moulding. During injection moulding, the feedstock is formed into the required shape by the application of heat and pressure. After solidification, the mould opens and demoulding takes place, that is, the green micro structured component is ejected from the mould cavity. The next step is debinding, where the binder is removed progressively from the green microstructured component. After debinding, the debound microstructured component is sintered to give the required properties.

As the required part features or details of micro PIM are down to the microns level, the binder, powder and associated processings have stricter requirements than for PIM. One important pre-requisite for successful micro PIM is a suitable binder which has to be mixed with an appropriate amount of powder (termed the powder loading) to form the feedstock. The binder must provide low viscosity for easy filling of the micro-cavities during injection moulding, high green strength for demoulding, as well as good shape retention and low shrinkage during debinding and sintering.[3–5] There is a need to specially tailored feedstock for micro PIM in order to exploit the full capability of the process as feedstocks based on conventional binder posed problems such as moulding limitations in filling micro-size structures and high aspect ratio, and the micro-

* Corresponding author. Tel.: +65 6790 6123; fax: +65 6791 1859.
E-mail address: jhmeng521@yahoo.com.cn (J. Meng).

0955-2219/$ – see front matter © 2010 Elsevier Ltd. All rights reserved.
doi:10.1016/j.jeurceramsoc.2010.11.034

size structures broke easily due to the relatively low green strength.[1,3,4,6]

To fabricate micro-components with small structural details, high sintered density, good surface finish and mechanical properties, fine particle size is preferred. Metal powder with mean particle size in the region of 1–5 μm seems suitable for many applications although better surface finish is achieved with finer particles.[7] In the case of ceramic powder where finer particle size is more easily available, there is a need to develop feedstocks from powder of submicron or nano-particle size in order to exploit the full potential of micro PIM. Processing such fine particle size, especially nano-particles, poses problems because of its large specific surface area and the associated tendency to agglomerate. With the use of finer particle size more binder is required to coat the surfaces of the particles and this can increase the final shrinkage after sintering. In a survey of available powders, only some powders are available in submicron particle size and some examples are copper, iron, tungsten, cobalt, zirconia, alumina and tungsten carbide.[8] The general rule is that the minimum feature that can be produced is ten times the particle size.[9] Thus, to produce smaller features or structural details, finer particle size is required. Debinding has to be performed carefully due to the use of finer particle size. This is because the spaces between the particles are extremely small and can promote crack formation during rapid debinding.[10] Decreasing the particle size by a factor of 100 from, for example, 20 um which is usual for PIM to 200 nm, increases the sintering stresses by a factor of 100. Therefore, to avoid distorting the micro-components during densification, sintering cycle includes long holding time at critical densification temperatures to accommodate the induced stresses and provide time for relaxation, before the temperature is ramped up again and new stresses are induced.[9]

Micro-channel parts are used in many micro-systems such as micro-reactor, micro-transducer, micro-fluidic device and micro-optics.[11,12] This paper covered the fabrication of alumina micro-channel part using submicron particle size of 170 nm. A specially formulated binder to accommodate the high specific surface area of the submicron powder was used. Different powder loadings were used in the study and a suitable powder loading was selected. Injection moulding, debinding and sintering of the micro-channel parts, and characterizations of the sintered micro-channel parts were conducted.

2. Experimental works

2.1. Materials

The submicron powder used in this work was high purity α-alumina powder (TM-DAR) supplied by Taimei Chemicals Co. Ltd of Japan. The powder was irregular in shape as shown in the micrograph (see Fig. 1) obtained from a field emission scanning electron microscope (JEOL FESEM JSM6700F). The average particle size was about 170 nm. The BET specific surface was measured using a BET Surface area analyser NOVA 1200 (Quantachrome) was 14.4 m^2/g. The density of the powder measured using an AccuPyc II 1340 pycnometer was 3.96 g/cm^3.

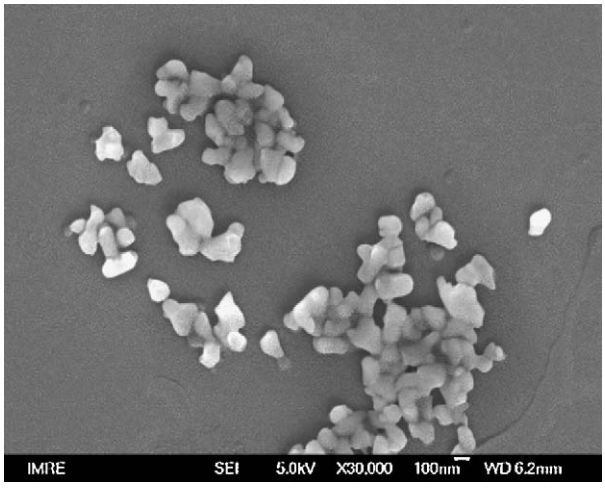

Fig. 1. FESEM micrograph of submicron alumina powder.

A multi-component binder, consisting of the following components was used: low density polyethylene (LDPE LL6201, ExxonMobil), ethylene vinyl acetate (EVA460, DuPont), paraffin wax (PW, MegaChem) and stearic acid (SA, Sigma–Aldrich). The composition of the binder in terms of weight ratio for LDPE:EVA:PW:SA is 35:30:25:10. The LDPE served as the backbone component. Thermal characterizations of the binder components were conducted to facilitate selection of suitable mixing conditions. Table 1 shows the thermal characteristics of the binder components. The highest melting temperature of the binder components measured on a Perkin-Elmer differential scanning calorimeter (DSC) model 7 was 126 °C for LDPE. The lowest start degradation temperature of the binder measured on a Perkin-Elmer thermogravimetric analyser (TGA) model 7 was 155 °C for SA.

2.2. Preparation of feedstock

Small-scale mixing of powder and binder components to form the feedstock was conducted on a Haake Rheocord 90 torque rheometer. From this small-scale mixing, the mixing behaviour and suitable powder loading can be established. The mixing of the feedstock was studied with 2 vol.% incremental powder

Table 1
Thermal characteristics of binder components.

Component	Melting temperature (°C)	Recrystallization temperature (°C)	Degradation temperature range (°C)
LDPE	126	102	410–520
EVA	85	64	290–520
PW	62	47	185–340
SA	77	55	155–302

loading, from 50 vol.% to 56 vol.%. Accordingly, the ratio of the weight of stearic acid (mg) to the surface area of the alumina powder (m^2), changed from 1.63 mg/m^2 to 1.28 mg/m^2. Based on the thermal characterizations of the binder components, the mixing temperature was set at 150 °C, above the highest melting temperature of 126 °C and below the lowest start degradation temperature of 155 °C. This would facilitate complete melting and prevent binder degradation. A mixing speed of 50 rpm was used. During mixing, the binder components were first fed in followed by the addition of one spoonful of powder per minute. Based on the mixing behaviour of the feedstocks for different powder loadings, a suitable powder loading of 52 vol.% (corresponding to 1.51 mg/m^2) was selected. Thermal characterizations and rheological testing were conducted on the selected feedstock.

The thermal degradation of the feedstock was evaluated by a Perkin-Elmer thermogravimetric analyzer (TGA) from 30 °C to 600 °C. The melting and re-crystallization temperatures of the feedstock were examined by a Perkin-Elmer differential scanning calorimetry (DSC) from 30 °C to 300 °C. For the TGA and DSC tests, the purging gas was nitrogen and a heating rate of 10 °C/min was used. A capillary rheometer (Göttfert 6000) was used to study the rheological behaviour of the selected feedstock. A die with 40 mm length and 1 mm diameter was used. Four temperatures, 130 °C, 140 °C, 150 °C and 160 °C, were selected for the rheological testings. The temperatures used were below the start degradation temperature of the feedstock.

2.3. Large-scale mixing

Based on the suitable powder loading established from small-batch mixing in a Haake Rheocord 90 torque rheometer and the resulting rheological results discussed in Section 3.3, large-scale mixing (to produce the feedstock for injection moulding) was conducted in a Hermann Linden Z-blade mixer. The powder and binder components were mixed at a temperature of 130 °C and mixing speed of 40 rpm. The binder components LDPE, EVA, PW, and SA were added into the mixer in the order indicated, followed by the addition of two spoonfuls of powder per minute. Finally, the feedstock was granulated into small pellets to facilitate injection moulding.

Table 2
Suitable injection moulding parameters for the micro-channel part.

Moulding parameters	Value
Injection stroke (mm)	17/13/12/10
Injection speed (%)	41/41/41/41/41
Injection pressure (MPa)	9.5
Follow-up pressure (MPa)	4
Melting temperature (°C)	160/160/160/150
Mould temperature (°C)	80

2.4. Injection moulding

The granulated feedstock was injection moulded into alumina micro-channel part on a Battenfeld 250 CDC horizontal injection moulding machine with a reciprocating screw. A two-plate mould with edge gate was used. A silicon mould insert with eleven micro-channels was used to mould the micro-channel part. A set of suitable injection moulding parameters used is shown in Table 2.

A (1 0 0) oriented silicon wafer was used to fabricate the silicon mould insert. The micro-channels were fabricated in a standard 8-in. silicon wafer by deep reactive ion etching (DRIE). The etched silicon wafer was then cut into smaller square dimensions of 6 mm × 6 mm where each cut square area has eleven micro-channels. The dimensions of each micro-channel as measured by a PLμ confocal profiler were a width of 200 μm and a depth of 135 μm. The length was 4 mm. The cut square silicon, namely the silicon mould insert, was mounted onto the circular cavity of the movable mould half. Fig. 2 shows the photograph of the movable mould half on the injection moulding machine

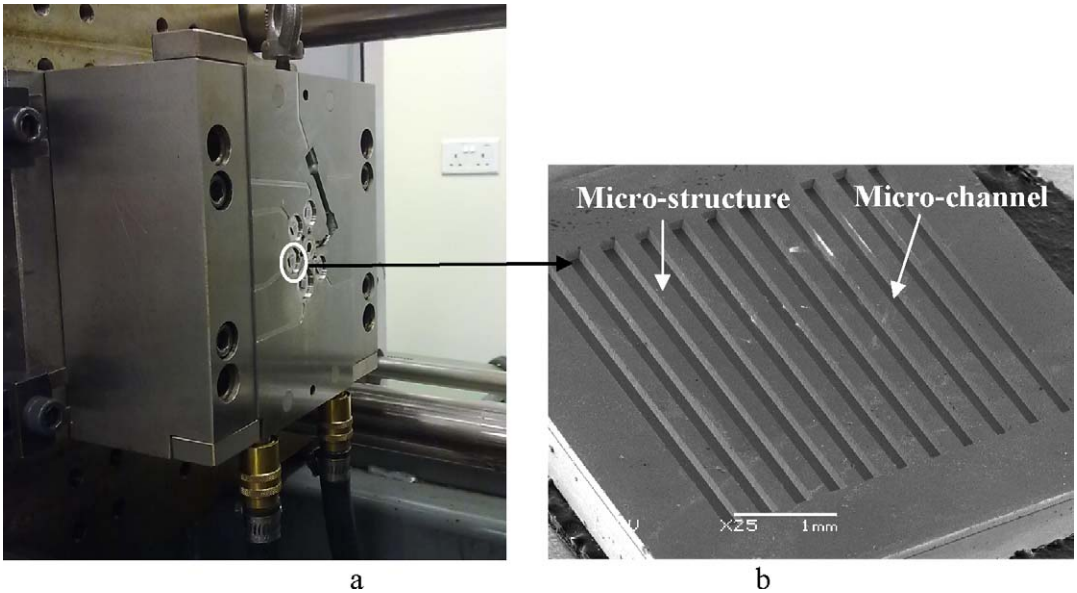

Fig. 2. (a) Photograph of the injection moulding machine and (b) SEM micrograph of the silicon mould insert.

and the micrograph of the silicon mould insert viewed under a JSM-5600LV scanning electron microscope (SEM).

2.5. Debinding and sintering

The moulded micro-channel parts were thermally debound in a Lindberg tube furnace with a mixture gas consisting of 95% argon and 5% hydrogen. Compared with the debinding atmosphere of air or oxygen, the mixture gas of argon and hydrogen can ensure a slower binder removal rate, which is beneficial to obtain defect-free and high strength part.[13,14] The thermal debinding was conducted according to a suitable debinding profile indicating temperature, time and heating rate. The debinding profile was based on earlier work for the 316L stainless steel feedstock.[15] The highest debinding temperature was set to 600 °C to ensure that all the binder components are removed and to facilitate handling. After debinding, pressureless sintering was conducted in a high temperature CM box furnace for five different sintering temperatures. A 5 °C/min heating rate to the sintering temperature and 60 min holding time at that temperature were used.

2.6. Characterization

The dimensions of the moulded, debound and sintered micro-channel parts were measured by a PLμ confocal profiler with an objective lens of 20× magnification. Measurements were conducted in six different locations on the micro-channels and micro-structures of the micro-channel part as shown in Fig. 3, and the average reported in this work. The diameter of the circular disc was measured. The densities of the sintered micro-channel parts were determined by using Archimedes's principle. The moulded and sintered micro-channel parts were examined under a JSM-5600LV scanning electron microscope. The sintered micro-channel parts were sectioned and then mounted in epoxy for the polishing of the cross-sections. The polished cross-sections were subjected to microhardness measurements. The Vickers microharness test with a load of 300 g was conducted on the base of the micro-channel part. The polished cross sections of the micro-channel parts were thermally etched in air, below the respective sintering temperatures, for 15–30 min. The etched cross-sections were observed using a field emission scanning electron microscope (LEO 1550).

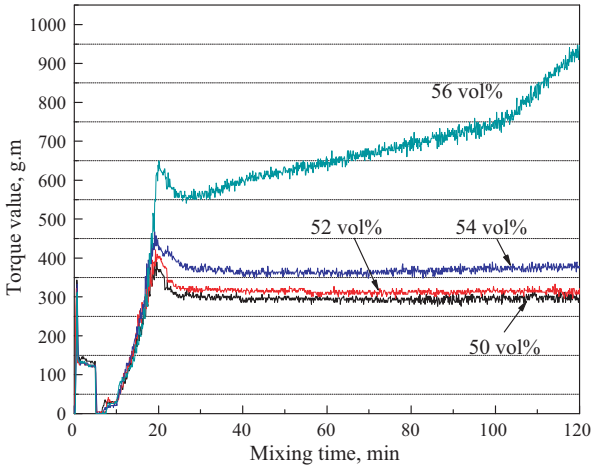

Fig. 4. Torque value versus mixing time for different powder loadings.

3. Results and discussions

3.1. Determination of suitable powder loading

During small batch mixing in a Haake mixer, the stability of the mixing torque with the mixing time is an indication of the homogeneity of the feedstock. Fig. 4 shows the torque versus mixing time for different powder loadings. In the first 10 min, all the binder components were added into the mixer. When powder was added into the mixer in small consecutive loadings, in the time duration between 10 and 20 min, the torque value increased significantly. After about 25 min of mixing, the torque reached a stable state, except for 56 vol.% powder loading. For 56 vol.% powder loading, the torque value increased significantly with the mixing time, indicating that the powder was not uniformly distributed within the binder. This was because the binder could not fill completely the voids between the particles and de-agglomeration of the powder took place during mixing. In the case of 54 vol.% powder loading, the torque stabilized

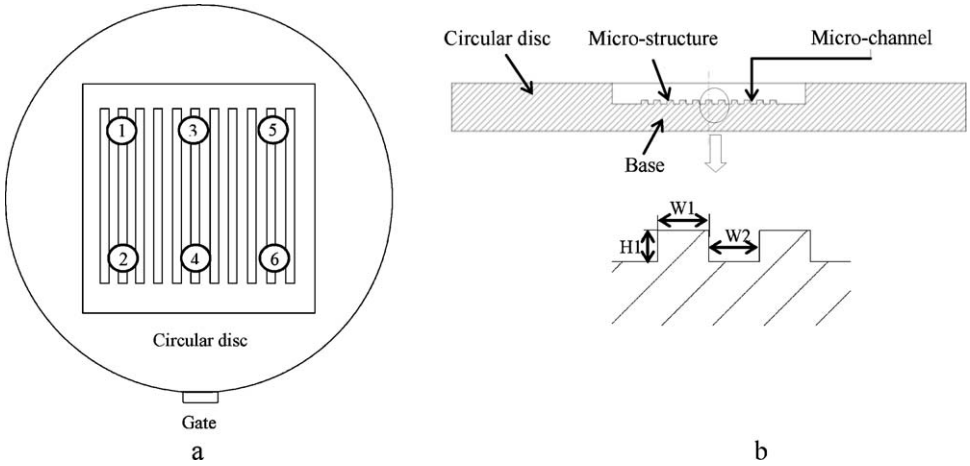

Fig. 3. (a) Top view and (b) cross section of locations of dimensional measurements for the micro-channel part.

initially but then increased slightly after 90 min of mixing. For 52 vol.% and 50 vol.% powder loadings, the torques were stable during mixing. However, lower powder loading can cause powder-binder separation during injection moulding and higher shrinkage during sintering. Hence, powder loading of 52 vol.% (corresponding to 1.51 mg/m^2) rather than 50 vol.% was selected to produce the feedstock for injection moulding.

3.2. Thermal properties

Fig. 5a shows the TGA curves of the multi-component binder and the individual binder components. From the TGA curves, one degradation step was found for LDPE, PW and SA. However, EVA degraded in two distinguishable steps, which was attributed to the elimination of side acetate group in vinyl acetate units followed by the chain scission of ethylene–acetylene copolymer at higher temperatures.[16] Similarly, the multi-component binder, which resulted from the mixing of the individual binder components, had also two distinct degradation steps. By comparison of the TGA curves, it was reasonable that the full degradation of PW and SA as well as the first degradation of EVA occurred in the first degradation temperature range (164–390 °C), whereas the degradation of LDPE and the subsequent degradation of EVA were at higher temperatures (425–520 °C). Above 520 °C, all the binder components were burned off. Based on the TGA result, a multi-step debinding profile was established to remove progressively the four binder components. The progressive debinding over a wide temperature range can help to retain the integrity of the microstructures and prevent the formation of debinding defects, such as blister, cracking and slumping. The TGA result also indicated that the temperatures for rheological testing and the feedstock temperature during injection moulding should be below the lowest degradation temperature of the binder components (that is, 164 °C) so as to prevent binder degradation.

As shown in Fig. 5b, three endothermic peaks at 56 °C, 70 °C and 119 °C and three exothermic peaks at 50 °C, 57 °C and 100 °C were present due to the melting and re-crystallization of the binder components. The peak at 56 °C was due to the overlapping melting of PW and SA. The peaks at 70 °C and 119 °C were due to the melting of EVA and LDPE, respectively. The melting temperatures of all binder components decreased after mixing with the alumina powder. This was probably due to the interfacial reactions between the powder and the binder components.[14] The mixing temperature, feedstock temperature during injection moulding and rheological test temperatures should be set higher than the highest melting temperature of 119 °C.

3.3. Rheological properties

Injection moulding depends on the feedstock (melt) viscous flow into the mould cavity, and this requires suitable rheological characteristic. The rheological testing temperatures were set higher than the highest melting temperature of 119 °C. Fig. 6 shows the apparent viscosity of the feedstock versus the shear rate for four testing temperatures: 130 °C, 140 °C, 150 °C and 160 °C. The apparent viscosity decreased with increasing temperature. This was attributed to powder loading volume reduction from larger expansion and disentanglement of the molecular chain during heating.[17] The feedstock exhibited pseudoplastic behaviour, that is, the apparent viscosity decreased with increasing shear rate. In practice, the maximum useful viscosity for a feedstock is 10^3 Pa s in the shear rate range between

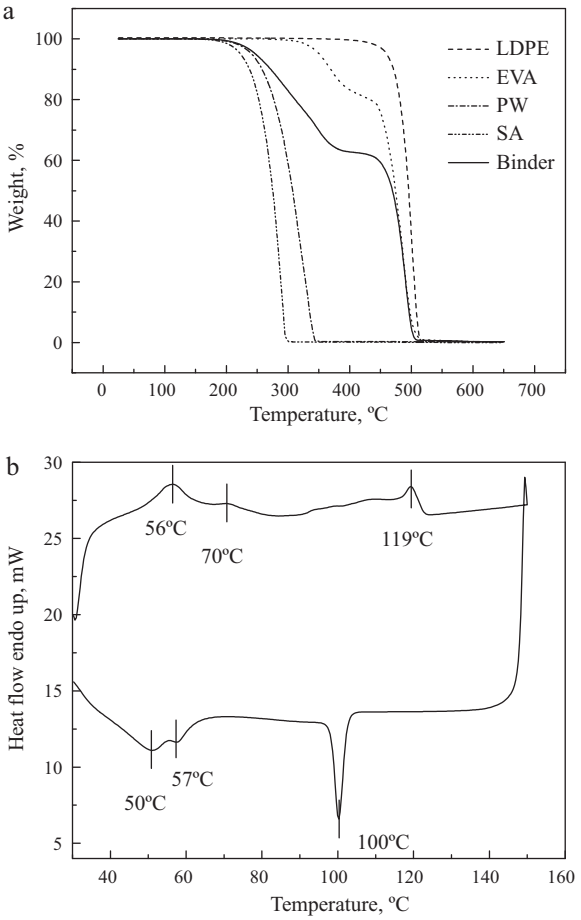

Fig. 5. (a) TGA curve of the binder and the binder components and (b) DSC curve of the feedstock.

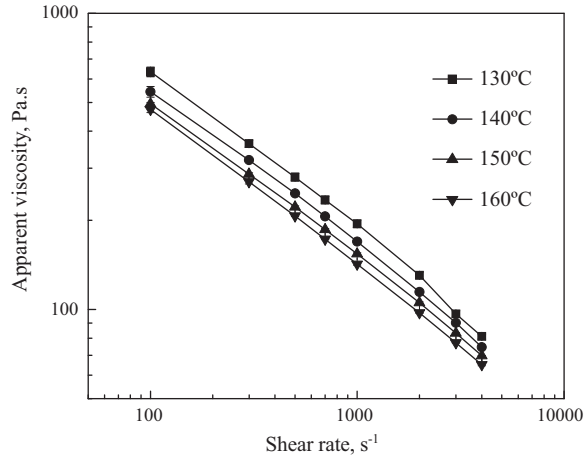

Fig. 6. Apparent viscosity of feedstock versus shear rate for different temperatures.

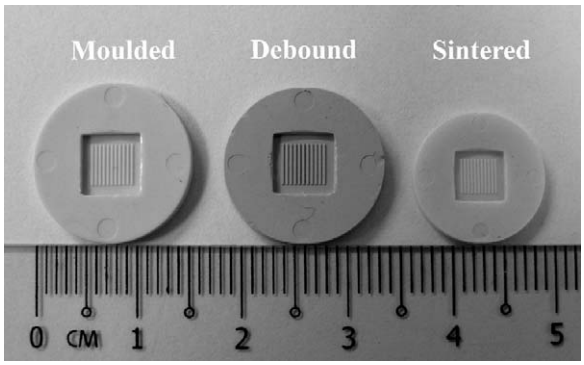

Fig. 7. Photograph of the micro-channel parts after different processing steps.

10^2 and $10^5\ s^{-1}$.[18] From Fig. 6, the feedstock is suitable for injection moulding.

3.4. Dimensional change and shrinkage

During thermal debinding and sintering, binder elimination and subsequent particles bonding take place, resulting in dimensional change of the PIM parts. The linear shrinkage of many PIM parts is in the range of 10% to 20%. However, for micro PIM parts, it can be above 20%.[19] Consequently, precise dimensional control of micro PIM parts will be more difficult as compared with PIM parts. Fig. 7 shows the photograph of the micro-channel parts after undergoing different processing steps. Compared with the moulded part, the dimensional change after debinding was not noticeable whilst the dimensional change after sintering was clearly evident. This was in agreement with the diameter change for the circular disc as shown in Fig. 8a. It can be seen that the apparent decrease in the diameter of the circular disc occurred after sintering.

Fig. 8b shows the average dimensions of the micro-channels and micro-structures of the micro-channel part after undergoing different processing steps. The dimensional changes in width and height of the micro-structures showed similar trend. Compared with the silicon mould insert, the width and height of the moulded micro-structures increased slightly. This was because the volumetric expansion due to cavity pressure decrement prevailed the volumetric shrinkage from cooling.[20] However, the width and height of the micro-structures tended to decrease slightly after debinding. The width and height of the micro-structures decreased gradually from sintering temperature of 1250 °C to 1350 °C. Above 1350 °C, the width and height of the micro-structures were relatively close. The width of the moulded micro-channels was smaller than that of the silicon mould insert. After debinding, the width of the micro-channels increased slightly. The width of the micro-channels decreased at sintering temperature 1250 °C, and then increased abruptly at 1350 °C.

The linear shrinkages ($\triangle L/Lo$) of the circular disc, the micro-channels and micro-structures of the micro-channel part at

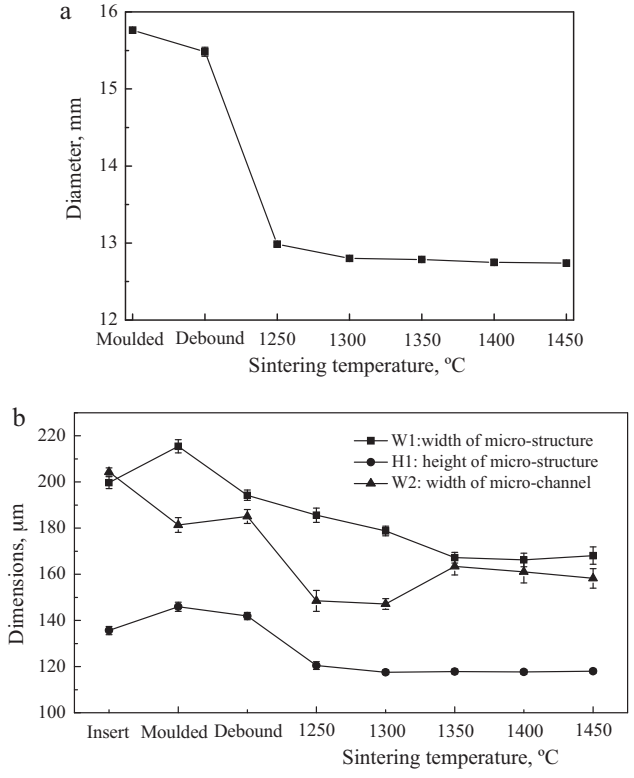

Fig. 8. Dimensions of (a) circular disc and (b) micro-channels as well as micro-structures after different processing steps.

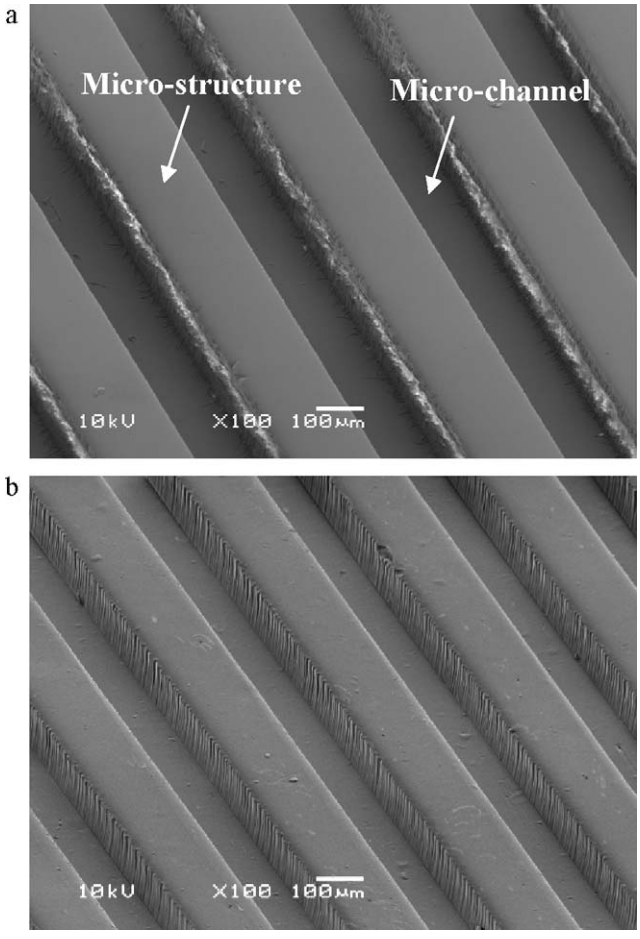

Fig. 9. SEM micrographs of the (a) moulded and (b) sintered micro-channel parts.

Table 3
Linear shrinkages of micro-channels, micro-structures and circular disc for different sintering temperatures.

Location	Sintering temperature (°C)				
	1250	1300	1350	1400	1450
Diameter of circular disc (%)	17.6	18.8	18.9	19.1	19.2
Width of micro-structure (%)	13.8	17.0	22.4	22.8	22.0
Height of micro-structure (%)	17.5	19.4	19.2	19.4	19.1
Width of micro-channel (%)	18.1	18.9	9.9	11.2	12.8

different sintering temperature are shown in Table 3. The shrinkage of the diameter of the circular disc was 17.6% at 1250 °C. In the temperature range between 1300 °C and 1450 °C, the shrinkages of the diameter were close, around 19%. The shrinkages of the width and the height of the micro-structure increased with sintering temperatures below 1350 °C. At 1350 °C and above, the shrinkages of the width and the height were independent of the sintering temperatures, and were about 22% and 19%, respectively. Noticeably, the shrinkages of the width of the micro-channels at 1350 °C and above decreased significantly compared with those at 1250 °C and 1300 °C. Actually, the shrinkages of the micro-channels were affected by the shrinkages of the micro-structures and the base. It was assumed that the shrinkage of the base was equivalent to that of the circular disc. Hence, the shrinkages of the micro-structures were higher than that of the base at 1350 °C and above, which led to the decrease in the shrinkages of the micro-channels.

3.5. Microstructure

Fig. 9 shows the SEM micrograph of the typical moulded and sintered micro-channel parts. Good shape retention without warpage and crack was achieved but the corners were slightly rounded. Fig. 10 shows the FESEM micrographs of the sintered micro-channel parts (at the base) at different sintering temperatures. Some pores between the alumina grains occurred below 1300 °C. At 1350 °C and above, the microstructures become denser and fewer tiny pores were found. The etched surfaces also revealed that the microstructures below 1300 °C

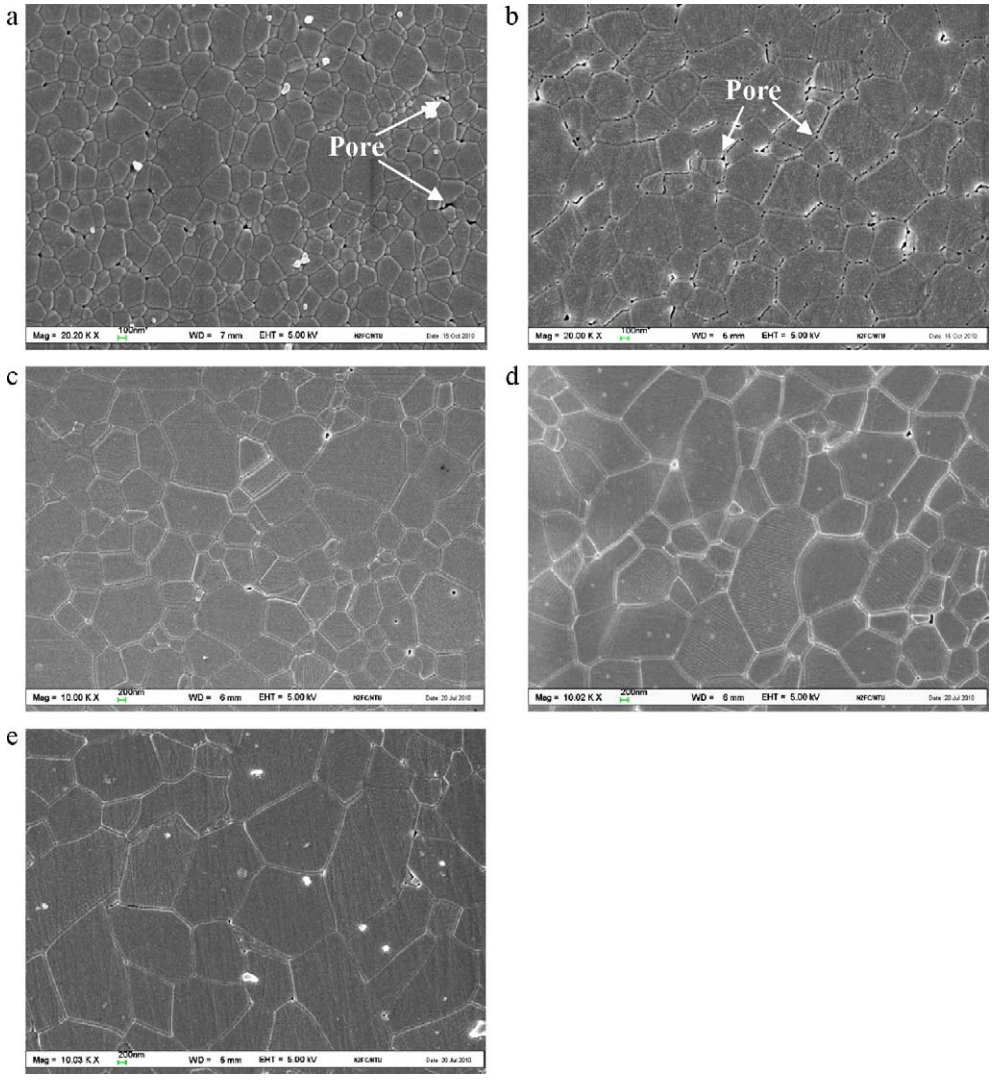

Fig. 10. FESEM micrographs of the sintered micro-channel parts for different sintering temperatures ((a) 1250 °C, (b) 1300 °C, (c) 1350 °C, (d) 1400 °C and (e) 1450 °C).

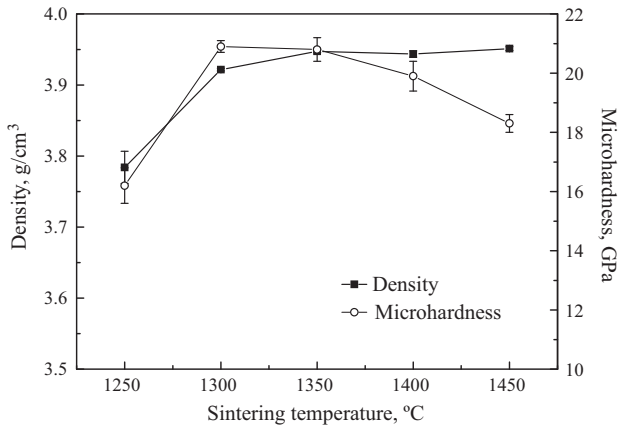

Fig. 11. Densities and microhardness of the sintered micro-channel parts for different sintering temperatures.

consisted mainly of equiaxed alumina grains. However, the microstructures at 1350 °C and above were inhomogeneous and some grains grew abnormally. Moreover, the microstructures consisted of equiaxed grains together with elongated grains, especially at 1400 °C and 1450 °C.

Fig. 11 shows the densities and microhardness (at the base) of the sintered micro-channel parts at different temperatures. No significant density change was observed for sintering temperatures of 1350 °C and above, which was in agreement with the result of the dimensional change discussed in section 3.4. The TM-DAR submicron alumina powder showed excellent sinterability because of its high specific surface area.[21] The TM-DAR alumina powder was easily densified at relatively low temperatures, and the relative densities of the sintered micro-channel parts were above 99% theoretical density at 1350 °C and above. The microhardness of the micro-channel parts at 1300 °C and 1350 °C were very close, which were the highest among all sintering temperatures. At higher temperatures of 1400 °C and 1500 °C, the microhardness decreased. According to the Hall–Petch relation, the larger grain sizes at 1400 °C and 1500 °C led to the decrease of the microhardness as compared to that for 1350 °C.

4. Conclusions

For the submicron alumina powder and binder components used, a suitable powder loading of 52 vol.% was established based on steady-state mixing torque and augmented by suitable rheological characteristics. Thermal and rheological characterizations of the feedstock enable the establishment of suitable processing conditions for the moulding and debinding of an alumina micro-channel part. Sintering was conducted at five different sintering temperatures. The micro-channel parts (after moulding, debinding and sintering processing steps) by micro PIM had good shape retention, without visible defects, such as warpage, incomplete filling and crack. The dimensions of the micro-channel parts changed with the different processing steps. High densification was achieved at 1350 °C and above. The microhardness of the micro-channel parts obeyed the Hall–Petch relation.

Acknowledgements

The authors would like to thank the Nanyang Technological University for awarding a research grant RGM 6/07 for this research work. The assistance rendered by Mr. Chen Beiming and Mr. Tan Wee Kiat is gratefully acknowledged.

References

1. Ruprecht R, Gietzelt T, Müller K, Piotter V, Haußelt J. Injection molding of microstructured components from plastics, metals and ceramics. *Microsyst Technol* 2002;**8**:351–8.
2. Petzoldt F. Micro powder injection moulding – challenges and opportunities. *Powder Injection Moulding Int* 2008;**2**:37–42.
3. Merz L, Rath S, Piotter V, Ruprecht R, Ritzhaupt-Kleissl J, Hausselt J. Feedstock development for micro powder injection molding. *Microsyst Technol* 2002;**8**:129–32.
4. Liu ZY, Loh NH, Tor SB, Khor KA, Murakoshi Y, Maeda R, et al. Micropowder injection molding. *J Mater Process Technol* 2002;**127**:165–8.
5. Liu ZY, Loh NH, Tor SB, Khor KA, Murakoshi Y, Maeda R. Binder system for micropowder injection molding. *Mater Lett* 2001;**48**:31–8.
6. Tay BY, Liu L, Loh NH, Tor SB, Murakoshi Y, Maeda R. Injection molding of 3D microstructures by μPIM. *Microsyst Technol* 2005;**11**:210–3.
7. Piotter V, Gietzelt T, Merz L. Micro powder-injection moulding of metals and ceramics. *Sādhanā-Acad Proc Eng Sci* 2003;**28**:299–306.
8. German RM. Materials for microminiature powder injection molded medical and dental devices. *Int J Powder Metall* 2010;**46**:15–8.
9. Zauner R. Micro powder injection moulding. *Microelectron Eng* 2006;**83**:1442–4.
10. Rota A, Imgrund P, Kramer L, Meyer R, Haack J, Micro. MIM approaches mass production. *Met Powder Rep* 2005;**60**:16–20.
11. Renaud L, Malhaire C, Kleimann P, Barbier D, Morin P. Theoretical and experimental studies of microflows in silicon microchannels. *Mater Sci Eng C* 2008;**28**:910–7.
12. Wu C, Atre SV, Whychell D, Park SJ, German RM. Nanoparticle building blocks for powder injection molded microsystems. In: *NSTI Nanotech 2007, Technical Proceedings*. 2007. p. 379–82.
13. Trunec M, Cihlář J. Thermal debinding of injection moulded ceramics. *J Eur Ceram Soc* 1997;**17**:203–9.
14. Lii DF, Huang JL, Lin CH, Lu HH. The effects of atmosphere on the thermal debinding of injection moulded Si_3N4 components. *Ceram Int* 1998;**24**:99–104.
15. Meng J, Loh NH, Tay BY, Fu G, Tor SB. Tribological behavior of 316L stainless steel fabricated by micro powder injection molding. *Wear* 2010;**268**:1013–9.
16. Trunec M, Cihlar J. Thermal removal of multicomponent binder from ceramic injection mouldings. *J Eur Ceram Soc* 2002;**22**:2231–41.
17. Liu L, Loh NH, Tay BY, Tor SB, Murakoshi Y, Maeda R. Mixing and characterisation of 316L stainless steel feedstock for micro powder injection molding. *Mater Charact* 2005;**54**:230–8.
18. German RM, Bose A. *Injection molding of metals and ceramics*. Princeton, NJ: Metal Powder Industries Federation; 1997.
19. Tay BY, Liu L, Loh NH, Tor SB, Murakoshi Y, Maeda R. Characterization of metallic micro rod arrays fabricated by μMIM. *Mater Charact* 2006;**57**:80–5.
20. Fu G. Development and analysis of micro powder injection molding. PhD Thesis. Singapore: Nanyang Technological University; 2008.
21. Echeberria J, Tarazona J, He JY, Butler T, Castro F. Sinter-HIP of α-alumina powders with sub-micron grain sizes. *J Eur Ceram Soc* 2002;**22**:1801–9.